Design and Simulation of Wideband, High Gain Matrix Antenna with Beam Steering and Low Side-Lobe Levels Features

Paul Karmann[1, *], Edson Martinod[2], Joël Andrieu[3], Mohamad Rammal[4]
[1]ITHPP, Drèle Thégra, 46317, France,
Email: paul.karmann@unilim.fr
[2]XLIM, University of Limoges, RF Systems, 7 rue Jules Vallès, 19100 Brive-la-Gaillarde, France,
Email: Edson.martinod@xlim.fr
[3]XLIM, University of Limoges, RF Systems, 7 rue Jules Vallès, 19100 Brive-la-Gaillarde, France,
Email: joel.andrieu@xlim.fr
[4]ITHPP, Drèle Thégra, 46317, France,
Email: mrammal@ithpp-alcen.fr
[*] *Corresponding author*

Abstract: **In this paper, a matrix antenna composed of radiating pixels elaborated in meta-materials is presented. The pixels are surmounted with a frequency selective structure and closed with four metallic walls. The cavity is excited by a radiating patch and filled with dielectric. This dielectric makes it possible to reduce the overall width of the pixel by increasing the dielectric length of the cavity while maintaining the performances of the pixel. The pixel is reduced to a width of 50.96 mm (0.34*λ) at 2 GHz. The -10 dB fractional bandwidth of the pixel is 22% (2-2.5 GHz). The pixel is then placed in a 17 elements matrix to achieve high steering angles. The optimization focuses on the steering capacity, the bandwidth and the side-lobes levels. On the whole band, the steering angle is more than 70° and the antenna achieves low side-lobes levels at less than -9.9 dB. A device to reduce the mutual coupling between the elements by using soft surfaces is also presented. These surfaces allow to widen the matching band while the steering is produced.**

Keywords: **Beam steering, Matrix antenna, Soft surfaces, Wideband antenna.**

I. INTRODUCTION

The demand for high gain antennas capable of achieving high steering angles is becoming more and more prevalent in civil and military applications. To reduce the need to use multiple antennas, wide bandwidth antennas are especially sought after. Among the antennas that can combine both wide bandwidth and high steering angles are the antennas using a radiating patch base. Patch antennas are known to have narrow bandwidth and some methods must be used to improve them. Among these methods we find the reconfiguration techniques allowing to achieve multiple resonances whether using P-i-N diodes [1] multiple ports [2] or phase shifters [3], non-rectangular patches [4], stacked structures [5] and cavity backed patches [6,7]. To achieve a high steering angle while conserving its gain, the antenna must also possess a high half-power beamwidth (HPBW). To achieve this, it is possible to use metal protrusion [8], metallic walls [9] or high impedance periodic structures [10].

One of the structures that combines both wide band with high HPBW is the Agile Radiating Matrix Antenna (ARMA) [11,12]. These antennas are composed of several joined elements called pixels which are low-profile and high gain and give to the matrix its characteristics. They can achieve fractional bandwidth of up to 40% [13,14] and their HPBW allows the matrix to achieve a high steering angle of up to 70° [15] in narrow band configuration while maintaining low side-lobe levels [16]. These characteristics make the ARMA technology a good choice for wide-band high steering antennas.

In their standard design, the pixels have a width of 0.5 λ_0, with λ_0 the wavelength of the low working frequency. This allows them to achieve a wide band but reduces their steering capacity in the high frequencies. Indeed, when high steering angles are achieved, it leads to the appearance of grating lobes which reduce the directivity of the matrix. This should be avoided to maintain the high gain of the matrix and the low side-lobes levels obtained at a high steering angle. To achieve low grating lobes, the distance between each pixel phase center must follow equation (1) [17]:

$$d_{max} = \frac{\lambda}{1 + \sin(\theta_{max})} \quad (1)$$

With θ_{max} the achieved steering angle and d_{max} the maximum distance between two phase centers to ensure the absence of grating lobes. The working frequency is given by the wavelength λ. In the ARMA matrix, the pixels form a contiguous surface. The distance between two phase centers is then the width of the antenna. For the application, the S band is required. The low frequency is then roughly 2 GHz which corresponds to λ=150 mm. To achieve a steering

The authors would like to thank the French Defense procurement Agency (DGA) for their founding.

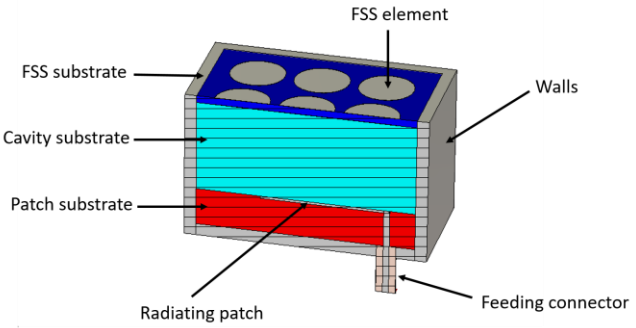

Fig. 1. Cut view of the pixel.

angle of 70°, the pixel needs to be at most 53 mm wide, which roughly corresponds to 0.35 λ_0. It has been shown in [18] that it is possible to slightly reduce the dimensions of the pixel with effects on the band and gain of the antenna but not on its other characteristics. The new dimensions may as such be smaller than what it needs to be with the modified band.

One of the main drawbacks that arise while using beam steering antennas is the coupling between them. Indeed, these interactions generally implies degradation of the return parameters of one or more antennas. One of the phenomena linked to these perturbations is the transition of surface current between the elements. Among the way to reduce their impact, it has been shown that moving the antennas apart reduce the impact of surface current [19]. However, this is not possible to achieve with the ARMA technology because of the radiating matrix properties of the antenna. Other solutions that can be used to reduce the impact of surface current generally revolves around corrugations [20], soft surfaces [21] or electronic bandgap (EBG) elements [20]. While the EBG structures present lots of interest, the main limitation of the utilization of filtering component in the ARMA technology is the available space between each element. As the soft structures are more compact at a given frequency [22], they have been privileged in this study.

The paper is organized as follows. The second section presents the proposed pixel which follows the dimensions set by the equation (1) and its performances are analyzed. The third section presents the performances of a matrix composed of the proposed pixels and the benefits of the reduction. The fourth section presents the problematic resulting from the mutual coupling in the matrix and the way it can be solved. Finally, the last section presents a summary and concluding remarks.

II. PROPOSED PIXEL DESIGN AND PERFORMANCES

The cut view of the pixel is shown in Fig. 1. The pixel is composed of a frequency selective surface (FSS) made from metallic elements placed on both sides of a substrate. The pixel is excited by a radiating patch which lies on a substrate and is fed by an SMA connector. The cavity is filled by a substrate and is closed by four electric walls. The geometric

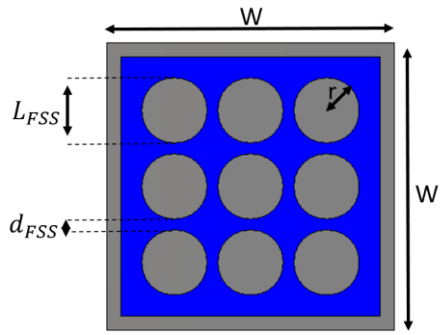

(a)

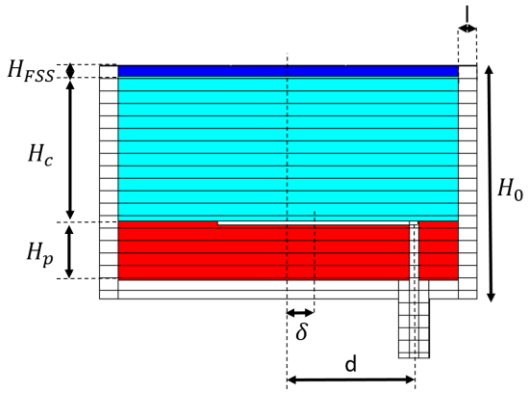

(b)

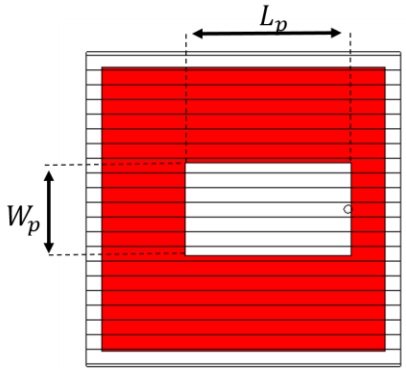

(c)

Fig. 2. Dimensional parameters of the pixel: (a) Top view of the FSS (b) Top view of the exciting patch. (c) Side view without walls.

TABLE I. GEOMETRICAL DIMENSIONS OF THE PIXEL

Parameter	Dimension (mm)	Parameter	Dimension (mm)
W	50.96	H_0	31.52
H_p	8	H_s	19.5
H_{FSS}	1.52		
W_p	15	L_p	27
d	13	δ	4
L_{FSS}	11.5	r	5.5
d_{FSS}	2		

dimensions are shown in Fig. 2 and the dimensions are presented in table I. The walls form a square structure with a width of W and a height h_0. The walls are 2.5 mm wide, which makes the inside of the cavity 45.96 mm wide. The patch substrate has a height of H_p and an ε_r=4.2, the cavity

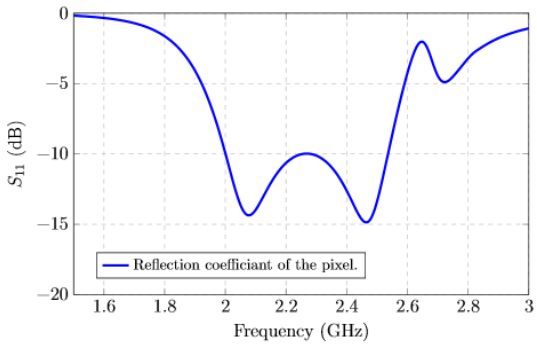

Fig. 3. Simulated reflection coefficient of the pixel.

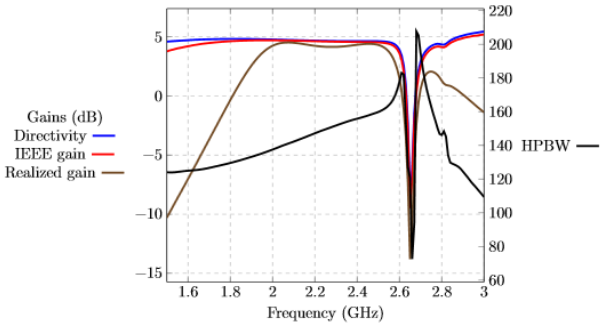

Fig. 4. Gains of the pixel over the whole frequency band.

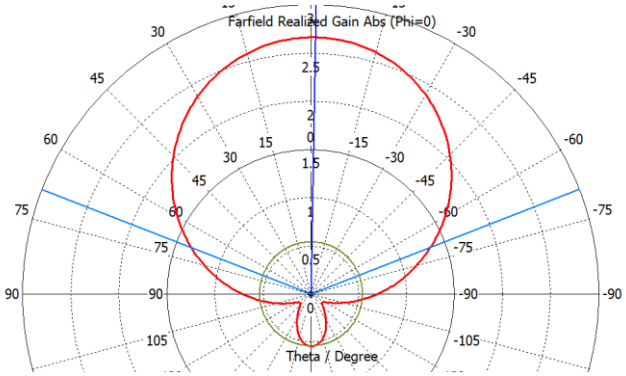

Fig. 5. Realized gain radiation pattern at 2 GHz

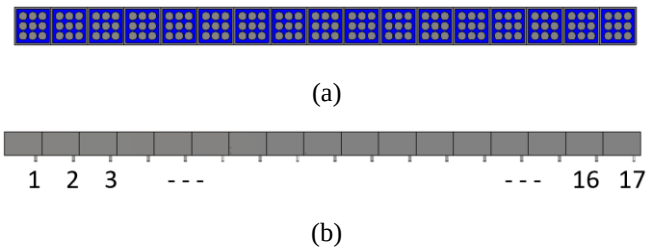

(a)

(b)

Fig. 6. Views of the matrix: (a) Top view. (b) Side view.

substrate has a height of H_s and an ε_r=3.2. The FSS substrate is a Rogers RO4003C substrate with a height of H_{FSS} and an ε_r=3.55. The GND plane makes up for the rest of the total height H_0 with a height of 2.5 mm. The size of the exciting patch is W_p x L_p. It is fed with a SMA connector placed at d from the center of the patch. The whole structure consisting of the patch and its connector is off-centered by δ. The elements of the FSS have a lateral dimension of L_{FSS} and a blend radius of r. Each element is separated from the other with a distance d_{FSS}. The central element of the FSS structure is located at the center of the pixel.

The dielectric of the patch substrate and the cavity are chosen as proof of concept for the antenna reduction and therefore are not existing materials. They both have a tan(δ)=0.0027 at 1 GHz. However, the Arlon AD 410 and Arlon AD 320 are both good candidates for the patch substrate and the cavity substrate respectively.

The antenna is simulated using CST Microwave Studio 2020 and the results are the following: the operating frequency band shown in Fig. 3 for the pixel is from 2 GHz to 2.5 GHz which corresponds to 22%. It is lower than the expected one of the pixels of 0.5 λ_0. This is due to the reduction of the pixel and the appearance of perturbations in the higher frequencies, starting at 2.55 GHz, which can be seen in the Fig. 4. They can be observed with the rapid increase followed by the reduction of the HPBW and the strong reduction of all the gains of the antenna. This negatively affects the radiating pattern in the high frequencies and is not suitable for steering applications.

The cavity filled with dielectric material allows for the pixel to achieve a lower width compared to other pixels using comparable frequency bands. Indeed, it allows to increase the electric length inside the cavity, offsetting the reduction of its width. This allows to better keep up with equation (1). Furthermore, the reduction of the width of the antenna pixel has a beneficial effect on the HPBW of the pixel which is increased for all the frequencies. The radiating pattern of the pixel is shown in Fig. 5 for the frequency 2 GHz. The HPBW is greater than 135° over the entire operating band which should make it possible to obtain a large steering angle. The increase of the HPBW causes a reduction of the gain of the pixel compared to a pixel with a lower HPBW. Indeed, the energy is spread over a wider area. In this configuration, the realized gain is 2.67 dBi at 2 GHz. The pixel reduction and geometric dimensional changes also cause a small shift in the main lobe direction of the pixel. This shift ranges from -0.8° at 2 GHz to -3.7° at 2.5 GHz. The maximum realized gain difference between the main lobe direction and the normal of the pixel is small and the main direction of the matrix composed of the pixels is unchanged by this variation, as such it is not a problem for the steering capacity of the antenna.

III. PROPOSED MATRIX ANTENNA DESIGN AND PERFORMANCE RESULTS

In order to demonstrate the steering capacity of the matrix antenna composed of the proposed pixels, a 17-elements matrix has been simulated. The matrix is presented in the Fig. 6. This number of elements has been chosen in order to allow a comparison with past results of the antenna which used the same number of elements [11].

The steering angle was obtained by shifting the feeding phases of the pixels. No changes were made on the amplitudes of the signals. The phases were shifted using the classic formula (2) [17]. With Φ the phase difference between two consecutive pixels, d the distance between each phase center, θ the steering angle and λ the wavelength of the working frequency.

TABLE II. SCANNING RADIATION PERFORMANCES AT DIFFERENT FREQUENCIES FOR DIFFERENT STEERING ANGLES

Frequency	2 GHz		2.25 GHz		2.5 GHz	
Steering angle (deg)	Gain (dBi)	SLL (dB)	Gain (dBi)	SLL (dB)	Gain (dBi)	SLL (dB)
-75	12.7	-9.9	13.3	-9.9	13.3	-10.0
-71	13.4	-11.4	14.1	-11.4	14.3	-11.7
-60	13.3	-12.9	14.1	-12.8	14.4	-12.7
-30	13.5	-12.9	15	-12.7	15.7	-12.8
0	13.8	-13.2	15.7	-13.3	16.8	-13.4
30	13.4	-12.8	15	-12.7	16	-12.7
60	13.3	-12.9	14.1	-12.8	14.4	-12.7
71	13.4	-11.5	14.1	-11.4	14.3	-11.9
75	12.7	-10.0	13.3	-9.9	13.2	-10.0

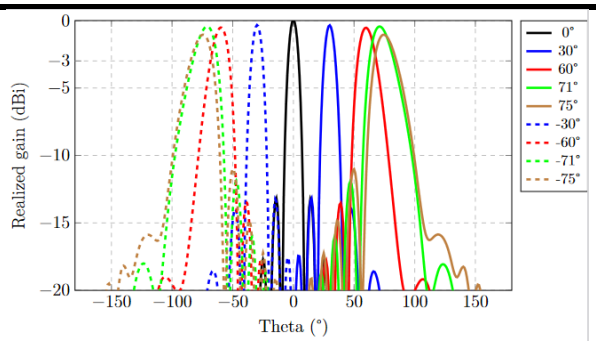

(a)

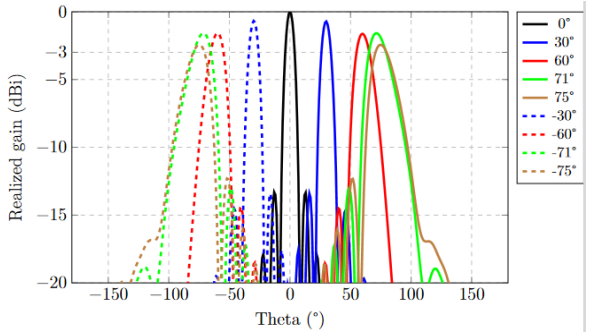

(b)

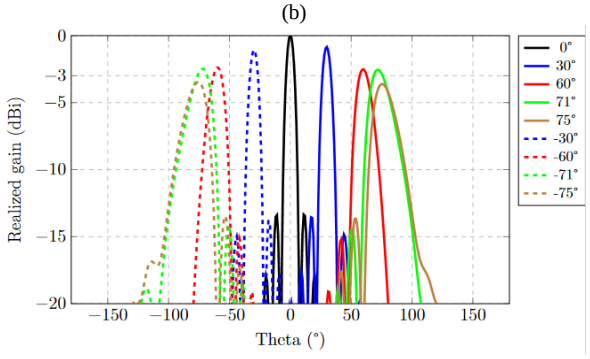

(c)

Fig. 7. Steering angle of the matrix for different frequencies: (a) 2 GHz normalized at 13.8 dBi (b) 2.25 GHz normalized at 15.7 dBi (c) 2.5 GHz normalized at 16.8 dBi

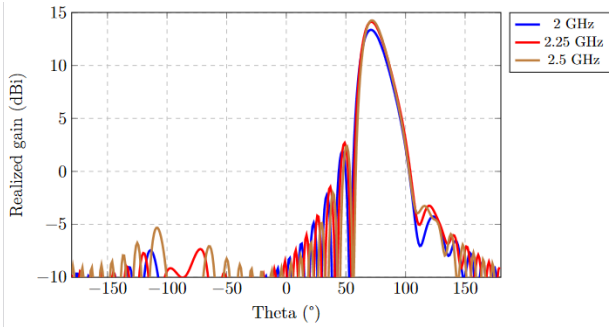

Fig. 8. Maximum steering angle for each frequency

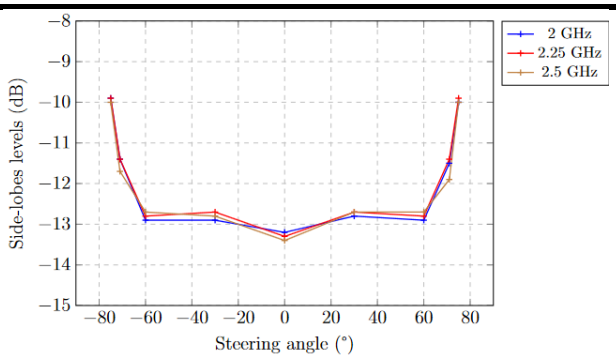

Fig. 9. Side-lobes levels for each frequency

$$\phi = \frac{360 * d * \sin(\theta)}{\lambda} \quad (2)$$

The scanning performances in the E-plane of the matrix are presented in Fig. 7 for three frequencies in its operating bandwidth. The beam can scan with a variation of less than 3 dB from -70° to +70° for the entire frequency band. Fig. 8 present the steering maximum achieved angle for the three frequencies while complying to the 3 dB criteria. The realized gain performances of the matrix are shown in Table II. The realized gain decreases with the steering angle. However, the back-lobes concur to the overall gain of the matrix after 60°. This allows to improve the gain and to stay within the 3 dB variation range. It is notably shown at the frequency of 2 GHz for which the gain at 71° is higher than that is achieved at 60°. The matrix also has low side-lobes levels (SLL) on the entire bandwidth with the highest ones being at -9.9 dB. The grating lobes are kept lower than -15 dB of the main lobes thus ensuring a high-quality beam steering. The SLLs for each frequency are presented in Fig. 9, they show a good similarity for each steering angle.

The Table III compares the steering results of this work and some other antennas. The papers presenting these antennas show that it is possible to achieve a high steering angle. However, these high angles tend to deteriorate either the SLLs or the bandwidth of the antenna. The proposed design, while not achieving the highest in each category, seems to present a good comprise between all parameters.

TABLE III. COMPARISON OF SCANNING PERFORMANCES BETWEEN THIS PAPER AND [1-3], [11] AND [23-26]

Reference	Relative BW	Peak SLL	Scan range
[1]	5%	-7.8 dB	150°
[2]	2%	-10.1 dB	144°
[3]	3.3%	-8.8 dB	162°
[23]	3%	-10 dB	150°
[24]	18%	-4.9 dB	144°
[25]	3%	-15 dB	140°
[26]	17%	-3 dB	180°
[11]	4%	-11 dB	140°
This work	22%	-9.9 dB	142°

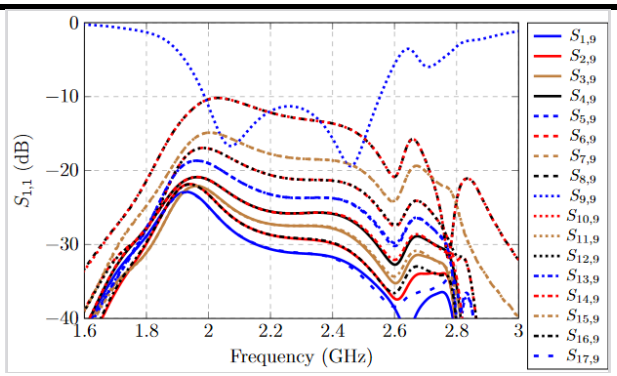

Fig. 10. Coupling coefficient of the 17-elements matrix without soft surfaces.

IV. MUTUAL COUPLING IN THE MATRIX AND ADDITION OF SOFT SURFACES

While the proposed matrix antenna is able to achieve a wide scanning angle, the size reduction of the elements has caused an increase of the mutual coupling of the pixels. Those coupling are presented in Fig. 10. In this figure, only the central pixel of the matrix is fed and the coupling are observed on the other elements. It allows to study the symmetry between both directions regarding the coupling coefficient. As such, the nearest pixels are the ones that are most affected. Those coupling cause the active reflection coefficient to go over -10 dB. This can be detrimental to the feeding used to power the matrix and reduce the gain of the antenna. To have a comparison base, the active adaptation parameters have been simulated for steering angle of 0°, 30° and 60°. They are presented in Fig. 11.

In order to decrease the coupling between the elements, a soft surface composed of metallic stripes on a substrate has been implemented. As the frequency most affected by the coupling is 2 GHz, this frequency has been chosen as a basis to reduce the impact of the coupling on it. The chosen solution is the addition of soft surfaces between each element. This causes the pixels to be slightly further apart, but the reduction of the dimensions of the pixels allows the matrix to still stay within the bounds set by equation (1). The geometry of the surface used is presented in Fig. 12. It is composed of three metallic stripes on a substrate with a depth that corresponds to formula (3) [21].

$$h = \frac{\lambda}{4 * \sqrt{\varepsilon}} \tag{3}$$

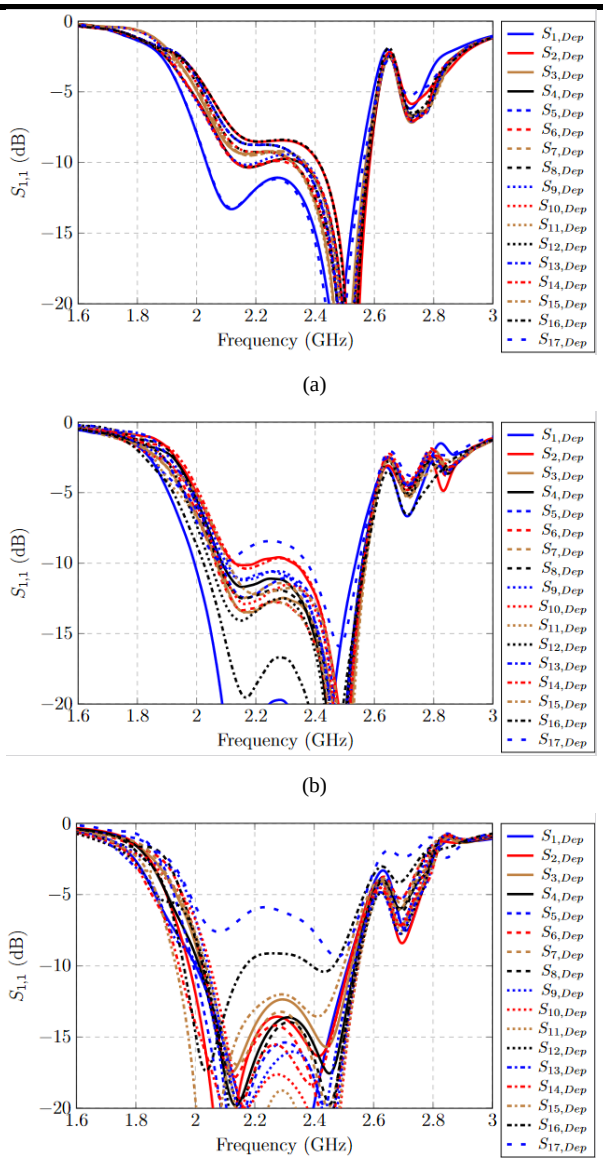

(a)

(b)

(c)

Fig. 11. Active adaptation parameters of the 17-elements matrix without soft surfaces for different steering angles: (a) 0° (b) 30° (c) 60°

With h the depth of the substrate, λ the wavelength that is filtered and ε_r the substrate permittivity. The distance between two walls of the new antenna is 5 mm. The substrate chosen to make the soft surfaces is an FR-4 substrate with a permittivity of 4.3. While this is a lossy substrate and as such is not desirable for soft surfaces because it reduce its performances [27], the simulations were made in order to consider a fabrication. The depth of the substrate is 18.08 mm and the metallic stripes have a width of 0.72 mm.

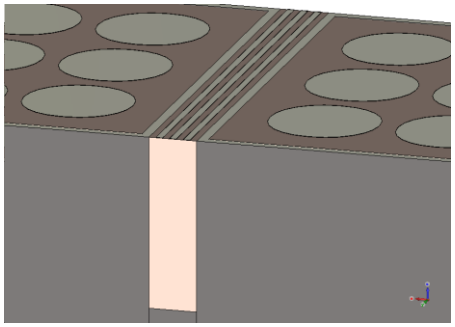

Fig. 12. View of the soft surface between the elements.

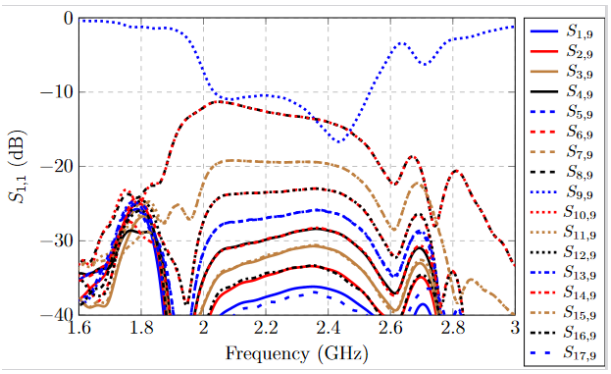

Fig. 13. Coupling coefficient of the 17-elements matrix with soft surfaces.

The coupling coefficient of a 17-elements matrix with these elements are presented in the Fig. 13. As with the matrix without the soft surfaces, they are computed on the central pixel, as they show a good symmetry the computed pixel does not matter much. Indeed, the results will be quite similar with another element being fed. They show an improvement of the coupling coefficient on all elements. The two closest elements, pixels number 8 and 10, go from a -10.1 dB maximum coupling to -11.3 dB. They are the pixels where the improvement is the least important. On the pixels 7 and 11, the coupling goes from -15 dB to -19.2 dB. It can be noted that, while the adaption parameter is changed, the overall performances of the matrix are improved. This is shown in Fig. 14 on which the active adaptation parameters of the matrix are shown. As with Fig. 11, the adaptation parameters are presented at a steering angle of 0°, 30° and 60°. In these figures, the benefits of the soft surfaces are made clearer. Indeed, they allow the antenna to achieve a far better band while no steering is applied. With this setup, the -10 dB adaptation band of the antenna is 2.05-2.55 GHz (which corresponds to a 21% fractional bandwidth).

While steering is applied, the soft surfaces allow the antenna to keep a larger band, albeit with a little more loss. The bandwidth of the new filtered antenna stays the same at a 60° steering angle but with a maximum a -6.5 dB. This is still far better than the previous antenna, that had its bandwidth drastically modified by the steering. At 30° the bandwidth is clearly improved in comparison with the previous antenna. For the higher steering angle however, the filtering elements are not enough to prevent disruption from the mutual coupling. This may stem from the fact that not all mutual coupling come from surface current.

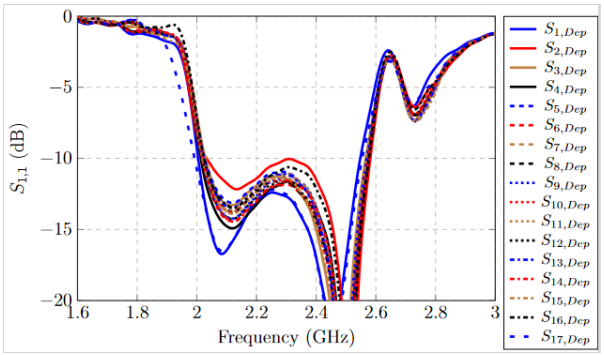

(a)

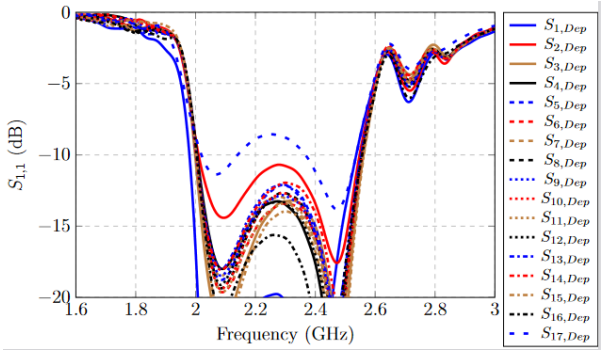

(b)

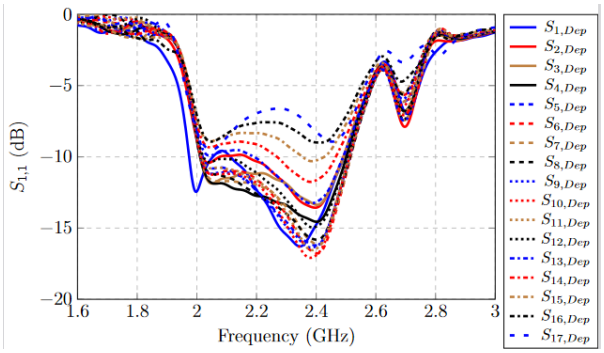

(c)

Fig. 14. Active adaptation parameters of the 17-elements matrix with soft surfaces for different steering angles: (a) 0° (b) 30° (c) 60°

It is also worth noting that a portion of the energy is diverted in the soft surfaces, and as such reduces the overall gain of the antenna. Indeed, at a 60° steering angle and 2 GHz, the reduced matrix achieves a 13.3 dBi realized gain. The reduced matrix with soft surfaces only has a 12.5 dBi gain. This difference is not present in the higher frequencies as the soft surfaces do not filter these. This reduction leads to the need to compromise between the bandwidth, the gain and the steering capacity in the design of future antennas. The radiating patterns of the matrix antenna are presented in Fig. 15 and the results are compiled in the Table IV. In this table it can be seen that the 3 dB steering capacity of the antenna is also slightly reduced from what it was without the soft surfaces. A comparison of the gains of the base antenna and the antenna using soft surfaces is presented Fig. 16. The deformation of the gain due to the back radiation is clearly visible in the figure. The new steering capacity is more around 130° over the whole band. It also has SLLs lower than -10.4 dBi in this steering range. A comparison between both antennas in term of evolution of SLLs is presented Fig. 17. This figure shows the breaking of the symmetry at 2 GHz which is the filtered frequency.

TABLE IV. SCANNING RADIATION PERFORMANCES OF THE MATRIX WITH SOFT SURFACE AT DIFFERENT FREQUENCIES FOR DIFFERENT STEERING ANGLES

Frequency	2 GHz		2.25 GHz		2.5 GHz	
Steering angle (deg)	Gain (dBi)	SLL (dB)	Gain (dBi)	SLL (dB)	Gain (dBi)	SLL (dB)
-75	9.31	-8.2	12.2	-9.2	12.3	-9.6
-65	11.8	-10.4	14.1	-12.2	14.1	-12.6
-60	12.4	-10.9	14.2	-12.3	14.2	-12.6
-30	14.1	-12.1	15.5	-12.7	15.9	-12.6
0	14.7	-12.8	16.2	-13.3	17	-13.3
30	14.2	-13.3	15.5	-12.8	16.1	-12.6
60	12.5	-12.5	14.2	-12.7	14.2	-12.6
65	12	-11.6	14.2	-12.6	14.1	-12.8
75	9.56	-9.9	12.2	-9.5	12.2	-9.6

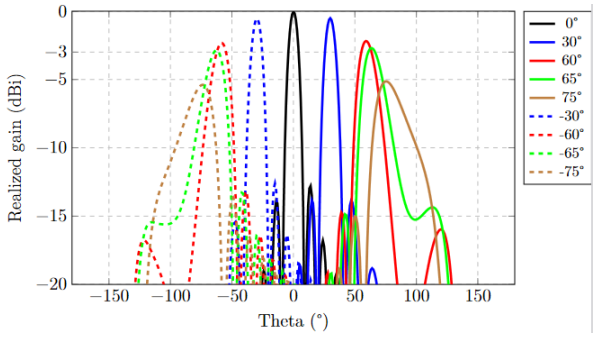

(a)

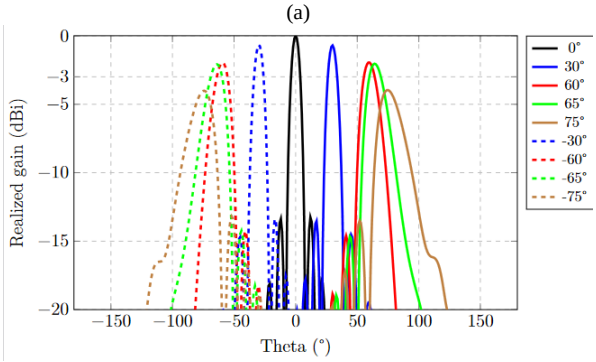

(b)

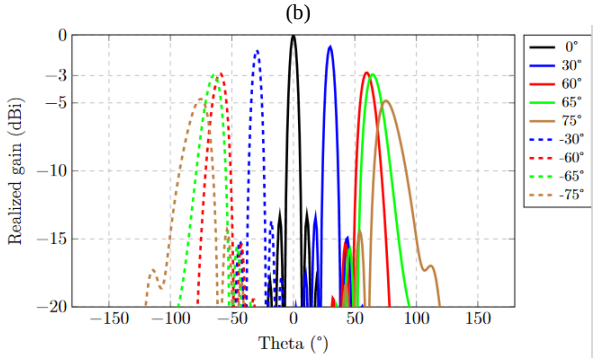

(c)

Fig. 15. Steering angle of the matrix for different frequencies: (a) 2 GHz normalized at 14.7 dBi (b) 2.25 GHz normalized at 16.2 dBi (c) 2.5 GHz normalized at 17 dBi

V. CONCLUSION

In this paper, an ARMA matrix composed of reduced pixels is studied. The pixels are composed of a radiating patch inside a cavity created by a frequency selective surface and filled with dielectric material. The use of such dielectric allows to obtain a reduced width of the pixel compared to the common design method and improves its half-power beam-width in the steering plane to more than 135°. The reduction of the pixel also leads to a reduction of the

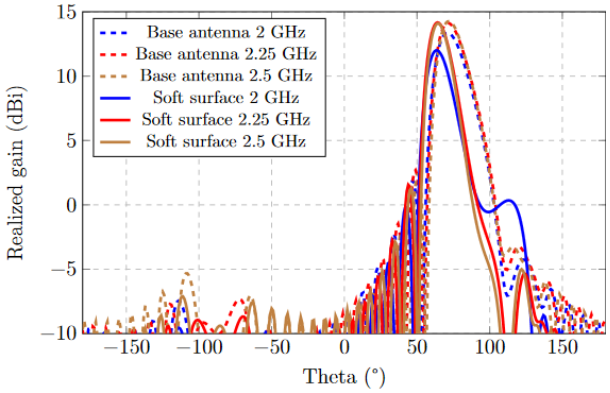

Fig. 16. Comparison between the maximum steering angle of the base matrix and the matrix with soft surfaces

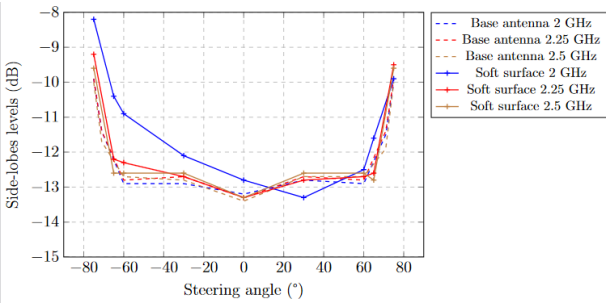

Fig. 17. Comparison between the side-lobes levels of the base matrix and the matrix with soft surfaces

matching and emission band, attaining a 22% fractional bandwidth. A matrix composed of 17 pixels then demonstrates its steering capacity. The matrix can scan from -71° to +71° with low side lobe levels and keep a stable gain over the on-scanning angles.

A method of reduction of the coupling coefficient between elements has then been studied. Allowing to improve the band while steering. It has still to be improved as it does not work as well in the higher steering angle and causes a loss of gain at the lowest one.

Further research on this topic will focus on the realization of a working prototype. This will demand the optimization of the pixels with mechanical requirement linked to the manufacturing process. It will also require the realization of a steering network to allow the measure of the active adaptation parameters.

REFERENCES

[1] X. Ding, Y. -F. Cheng, W. Shao and B. -Z. Wang, "A Wide-Angle Scanning Phased Array with Microstrip Patch Mode Reconfiguration Technique," *IEEE Transactions on Antennas and Propagation*, vol. 65, no. 9, pp. 4548-4555, 2017, DOI: 10.1109/TAP.2017.2722825.

[2] Y. -F. Cheng, X. Ding, W. Shao and B. -Z. Wang, "Planar Wide-Angle Scanning Phased Array with Pattern-Reconfigurable Windmill-Shaped Loop Elements," *IEEE Transactions on Antennas and Propagation*, vol. 65, no. 2, pp. 932-936, 2017, DOI: 10.1109/TAP.2016.2632736.

[3] Z. Chen, Z. Song, H. Liu, X. Liu, J. Yu and X. Chen, "A Compact Phase-Controlled Pattern-Reconfigurable Dielectric Resonator Antenna for Passive Wide-Angle Beam Scanning," *IEEE Transactions on Antennas and Propagation*, vol. 69, no. 5, pp. 2981-2986, 2021, DOI: 10.1109/TAP.2020.3030549.

[4] A. A. Deshmukh, A. A. Desai, P. Kadam and K. P. Ray, "Ultra-wide band E-shaped patch antenna," *2016 IEEE Annual India Conference (INDICON)*, 2016, pp. 1-5, DOI: 10.1109/INDICON.2016.7839154.

[5] C. Yang, S. Feng and S. Liu, "Microstrip Aperture-Coupled Stacked Patch Antenna Array for Wide-Band Wide-Angle-Scan Applications," *2018 Asia-Pacific Microwave Conference (APMC)*, 2018, pp. 594-596, DOI: 10.23919/APMC.2018.8617397.

[6] W. Zou, S. Qu and S. Yang, "Wideband Wide-Scanning Phased Array in Triangular Lattice with Electromagnetic Bandgap Structures," *IEEE Antennas and Wireless Propagation Letters*, vol. 18, no. 3, pp. 422-426, 2019, DOI: 10.1109/LAWP.2019.2893174.

[7] M. H. Awida, A. H. Kamel and A. E. Fathy, "Analysis and Design of Wide-Scan Angle Wide-Band Phased Arrays of Substrate-Integrated Cavity-Backed Patches," *IEEE Transactions on Antennas and Propagation*, vol. 61, no. 6, pp. 3034-3041, 2013, DOI: 10.1109/TAP.2013.2251595.

[8] S. Ye, X. Liang, J. Geng and R. Jin, "Wideband wide-slot antenna array with protrusion for wide-angle scanning," *2017 IEEE International Symposium on Antennas and Propagation & USNC/URSI National Radio Science Meeting*, 2017, pp. 1309-1310, DOI: 10.1109/APUSNCURSINRSM.2017.8072697.

[9] G. Yang, J. Li, R. Xu, Y. Ma and Y. Qi, "Improving the Performance of Wide-Angle Scanning Array Antenna with a High-Impedance Periodic Structure," *IEEE Antennas and Wireless Propagation Letters*, vol. 15, pp. 1819-1822, 2016, DOI: 10.1109/LAWP.2016.2537850.

[10] B. Ji and G. Yang, "Wide-Angle Scanning Phased Array Antenna," *2019 IEEE International Symposium on Antennas and Propagation and USNC-URSI Radio Science Meeting*, 2019, pp. 2065-2066, DOI: 10.1109/APUSNCURSINRSM.2019.8889234.

[11] H. Abou Taam, M. Salah Toubet, T. Monediere, B. Jecko and M. Rammal, "A New Agile Radiating System Called Electromagnetic Band Gap Matrix Antenna," *International Journal of Antennas and Propagation*, vol. 2014, Article ID 342518, pp. 1-7, 2014. DOI:10.1155/2014/342518.

[12] B. Jecko, E. Arnaud, H. Abou Taam and A. Siblini, "The ARMA concept: comparison of AESA and ARMA technologies for agile antenna design," *FERMAT Journal ART*, vol. 20, 2017.

[13] M. Salah Toubet, H. Abou Taam, B. Jecko and M. Rammal, "1D Ultra Low-Profile (ULP) EBG matrix for radar applications," *2013 IEEE Radar Conference (RadarCon13)*, 2013, pp. 1-4, DOI: 10.1109/RADAR.2013.6586043.

[14] M. Rammal, M. Majed, E. Arnaud, J. Andrieu and B. Jecko, "Small-Size Wide-Band Low-Profile "Pixel Antenna": Comparison of Theoretical and Experimental Results in L Band", *International Journal of Antennas and Propagation*, vol. 2019, Article ID 3653270, 8 pages, 2019. https://doi.org/10.1155/2019/3653270.

[15] H. Abou Taam, G. Zakka El Nashef, B. Jecko and M. Rammal, "Agile radiating matrix antenna system for radar applications," *2014 International Radar Conference*, 2014, pp. 1-4, DOI: 10.1109/RADAR.2014.7060438.

[16] H. Abou Taam, M. Salah Toubet, T. Monediere, B. Jecko and M. Rammal, "Interests of a 1D EBG Matrix compared to a patch array in terms of mutual coupling and grating lobe," *2013 7th European Conference on Antennas and Propagation (EuCAP)*, 2013, pp. 1045-1048.

[17] S. Drabowitch, A. Papiernik, H. Griffiths, J. Encinas and B. L. Smith, *Modern antennas*. Springer Science & Business Media, 2010, ch Array.

[18] M. Themalil, M. Majed, M. Rammal, E. Martinod and B. Jecko, "Miniaturized Pixel Antenna for Implantation on the ARGOS CubeSat 4U," *2019 IEEE-APS Topical Conference on Antennas and Propagation in Wireless Communications (APWC)*, 2019, pp. 154-156, DOI: 10.1109/APWC.2019.8870501.

[19] B. Abbasi Arand, A. Bazrkar and A. Zahedi, "Design of a Phased Array in Triangular Grid with an Efficient Matching Network and Reduced Mutual Coupling for Wide-Angle Scanning," *IEEE Transactions on Antennas and Propagation*, vol. 65, no. 6, pp. 2983-2991, 2017, DOI: 10.1109/TAP.2017.2690903.

[20] D. Sievenpiper, Lijun Zhang, R. F. J. Broas, N. G. Alexopolous and E. Yablonovitch, "High-impedance electromagnetic surfaces with a forbidden frequency band," *IEEE Transactions on Microwave Theory and Techniques*, vol. 47, no. 11, pp. 2059-2074, 1999, DOI: 10.1109/22.798001.

[21] P.-S. Kildal and A. Kishk, "Em modeling of surfaces with stop or go characteristics-artificial magnetic conductors and soft and hard surfaces," *Applied Computational Electromagnetics Society Journal*, vol. 18, no. 1, pp. 32-40, 2003

[22] E. Rajo-Iglesias, O. Quevedo-Teruel and L. Inclan-Sanchez, "Design considerations in planar soft surfaces," *2008 Loughborough Antennas and Propagation Conference*, 2008, pp. 289-292, DOI: 10.1109/LAPC.2008.4516923.

[23] Y. -F. Cheng, X. Ding, W. Shao, M. -X. Yu and B. -Z. Wang, "2-D Planar Wide-Angle Scanning-Phased Array Based on Wide-Beam Elements," *IEEE Antennas and Wireless Propagation Letters*, vol. 16, pp. 876-879, 2017, DOI: 10.1109/LAWP.2016.2613130.

[24] Y. Wen, B. Wang and X. Ding, "Wide-Beam SIW-Slot Antenna for Wide-Angle Scanning Phased Array," *IEEE Antennas and Wireless Propagation Letters*, vol. 15, pp. 1638-1641, 2016, DOI: 10.1109/LAWP.2016.2519938.

[25] Y. Cheng, X. Ding, W. Shao and C. Liao, "A High-Gain Sparse Phased Array With Wide-Angle Scanning Performance and Low Sidelobe Levels," *IEEE Access*, vol. 7, pp. 31151-31158, 2019, DOI: 10.1109/ACCESS.2019.2901721.

[26] G. Yang, Q. Chen, J. Li, S. Zhou and Z. Xing, "Improving Wide-Angle Scanning Performance of Phased Array Antenna by Dielectric Sheet," *IEEE Access*, vol. 7, pp. 71897-71906, 2019, DOI: 10.1109/ACCESS.2019.2919265.

[27] C. Wang, D. Bisharat, S. Kim, E. Li and D. F. Sievenpiper, "Simulation Analysis of Electromagnetic Surface Wave Suppression by Soft Surfaces, Including Effects of Resistive and Active Elements," *IEEE Antennas and Wireless Propagation Letters*, vol. 17, no. 12, pp. 2394-2398, 2018, DOI: 10.1109/LAWP.2018.2876332.